A 6n-Order Low-Frequency Mathematical Model of Multiple Inverters Based Microgrid

Wei Zhao, Erdong Chen, Xiaofeng Sun, *Member, IEEE* and Lei Qi
(Invited)

***Abstract*—Microgrid stability analysis is a critical issue especially due to the inverters' low-inertia nature. The voltage and current control loops influences on stability are researched frequently most of which focus on medium and high-frequency characteristic. Although the complete state-space model aims at low-frequency characteristic, it is too complicated and the calculation amount is huge with the scale of the microgrid increasing. One available reduced-order model of an inverter is simple, but it is suitable for only single inverter without network dynamic in microgrid. To fill in these gaps, a novel modeling method is proposed in this paper to investigate the low-frequency instability phenomenon and describe the whole DG connected system including network. In consideration of the high penetration level of induction motor (IM) loads and constant power (CP) loads in practical applications, the low-frequency mathematical model of IM and CP loads on the basis of static load is also built in this paper. Simulation and experimental results verify the effectiveness of the proposed model.**

***Index Terms*—Constant power (CP) load, droop control, low-frequency stability, induction motor (IM) load, microgrid, modeling.**

I. INTRODUCTION

MORE and more DG units are parallel operation to form a microgrid with the characteristic of plug and play[1-2]. And droop control is a commonly used strategy [3-5]. However, due to the negligible physical inertia of the inverters which makes the system vulnerable to oscillation resulting from network disturbances as well as their interaction. Therefore the research of stability on islanding microgrid is critical. The stability issues in microgrid can be divided into three parts that are low-frequency, medium frequency, high frequency characteristic according to the reason caused the instability phenomenon by frequency domain. On the base of neglecting outer power loop influence of the inverter, an impedance based stability criterion is modeled by its thevenin equivalent circuit in [6-9], which focus on the medium and high-frequency stability research.

To study the low frequency characteristic, small signal stability analysis method is widely used since it is easy to predict the system response when parameters are changed [10]. A modeling method is proposed in [11] and [12] which completely model the whole system not only including the characteristic of voltage and current loop, the power loop, the load, but also the utility grid. Thus, it is accurate to analyze the system stability and frequency domain characteristic from low frequency to high frequency range. The main difficulty of modeling the multi-inverters based microgrid with this method is that its order is high, results in a great number of parameters to be calculated and sufficiently capacious computer is demanded to do simulation.

To solve the problem of complexity mathematical model, the concept of reduced-order model for inverters in microgrid is studied. Low-frequency model is quite sensitive to the loads and power loop controller parameters for a microgrid connected inverter [13], while medium and high frequency models are mainly determined by the inverter's inner voltage and current control loops and the filters as well as load dynamics. A modeling method without considering the voltage and current controllers to simplify the mathematical model is proposed which can be used to study low-frequency instability [14-18]. However, this modeling method just fit for one single inverter and it can't be applied for multiple inverters based microgrid. The stability characteristic of multi-inverters microgrid is not guaranteed by the inherent stability and functionality of an individual inverter [6].

Aiming at the above issues, this paper focuses on how to build a reduced-order model for a microgrid considering the inverters, static loads and line impedances. A novel 6n-order mathematical model where n represents the number of inverters in the microgrid is set up for the microgrid feeding static loads. The order of proposed model is far less than the full order model in [11] and [12], and the low-frequency model is suitable for the multi-inverters connected microgrid stability analysis. Since rotor oscillations of an inductance motor (IM) yield both

Manuscript was submitted for review on 24, August, 2018.
This work was supported by the National key research and development plan 2016YFB0900300, National Natural Science Foundation of China under Grant51677162 and Natural Science Foundation of Hebei Province E2017203337
Wei Zhao is with Key Laboratory of Power Electronics for Energy Conservation and Motor Drive of Hebei Province, Yanshan University, China (e-mail: zwysu@ ysu.edu.cn).
Erdong Chen, was with Yanshan University, Qinghuangdao, Hebei, 066004 China. She is now with the Delta, Shanghai, China (e-mail: chenerdonh890731@163.com)
Xiaofeng Sun is with Key Laboratory of Power Electronics for Energy Conservation and Motor Drive of Hebei Province, Yanshan University, China (e-mail: sxf@ysu.edu.cn).
Lei Qi is with Key Laboratory of Power Electronics for Energy Conservation and Motor Drive of Hebei Province, Yanshan University, China (e-mail: qil@ysu.edu.cn).
Digital Object Identifier 10.30941/CESTEMS.2018.00033

mechanical and electrical power oscillations, the output power of an individual DG unit feeding an IM inherently contains the frequency modes of these oscillation [19]. The CP loads present to be a negative incremental resistance which may lead to a degradation of small-signal damping [20], [21]. This paper also proposes a 6n+3-order and 6n-order mathematical model to analyze the low-frequency characteristics of IM and CP loads respectively, where n also represents the number of inverters.

II. Proposed 6n-order Model Of An Autonomous Microgrid With Static Loads

A microgrid system composed of "n" inverters whose input power supplied by microsources, such as fuel cells, PV units, dc storages, and so on. All the units are connected to the point of common coupling (PCC), as shown in Fig. 1(a). Fig. 1(b) is a three-phase VSI with LC filter working in islanding mode and controlled by conventional droop control strategy. *L*f, *R*f and *C*f are three-phase LC filters. *L*c and *R*c are line impedances. i_{Labc}, E_{abc} and i_{abc} are inverter-side currents, filter capacitor voltages and output currents of the inverter respectively.

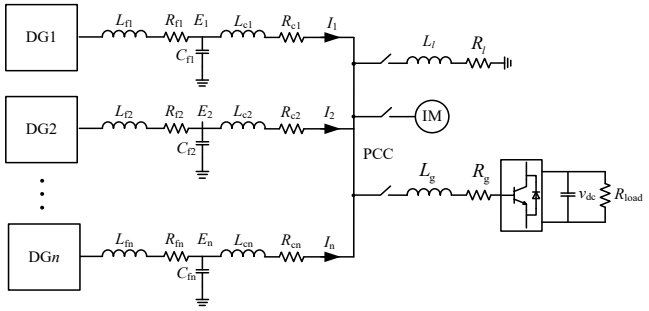

(a) Stand-alone microgrid with "n" inverters

(b) Schematic diagram of three-phase VSI with LC filter.

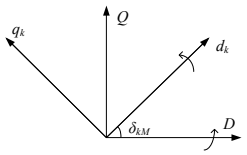

(c) Reference frame transformation.

Fig. 1. Structure block diagram and frame transformation.

Based on this structure, the bandwidth of the closed-loop transfer function of the current loop and voltage loop is around 1000Hz [22]. The active power-frequency droop and reactive power-voltage magnitude droop closed-loop transfer functions are proposed in [23]. The bandwidth of outer power loop is around 5Hz. The inner voltage and current control bandwidth is much higher than that of the outer power control, so the reduced-order model can be developed by neglecting the inner loops.

Firstly, only a static load will be considered. For the microgrid with n inverters, a synchronous D-Q frame from anyone of the all inverters is chosen as the common reference frame which is showed in Fig. 1(c). Here, δ_{kM} is the angle of the reference frame of *k*th inverter with the common reference frame of *M*th inverter. The relationship between D-Q axis and d-q axis is shown in (1).

$$[x_{DQM}] = T_{skM} \cdot [x_{dqk}] \tag{1}$$

Where

$$T_{skM} = \begin{bmatrix} \cos(\delta_{kM}) & -\sin(\delta_{kM}) \\ \sin(\delta_{kM}) & \cos(\delta_{kM}) \end{bmatrix} \tag{2}$$

The small signal equation of (1) is shown in (3).

$$[\Delta x_{DQM}] = T_{skM} \cdot [\Delta x_{dqk}] + T_{ckM} \cdot [\Delta \delta_{kM}] \tag{3}$$

Where

$$T_{ckM} = \begin{bmatrix} -X_{dk}\sin(\delta_{kM}) - X_{qk}\cos(\delta_{kM}) \\ X_{dk}\cos(\delta_{kM}) - X_{qk}\sin(\delta_{kM}) \end{bmatrix} \tag{4}$$

If there are n inverters, (5) can be obtained.

$$\begin{bmatrix} \Delta i_{DQ1} \\ \Delta i_{DQ2} \\ \vdots \\ \Delta i_{DQn} \end{bmatrix} = T_1 \begin{bmatrix} \Delta i_{dq1} \\ \Delta i_{dq2} \\ \vdots \\ \Delta i_{dqn} \end{bmatrix} + T_2 \begin{bmatrix} \Delta \delta_{1M} \\ \Delta \delta_{2M} \\ \vdots \\ \Delta \delta_{nM} \end{bmatrix} \tag{5}$$

Where

$$T_1 = \begin{bmatrix} T_{s1M} & & & \\ & T_{s2M} & & \\ & & \ddots & \\ & & & T_{snM} \end{bmatrix}_{2n\times 2n} \quad T_2 = \begin{bmatrix} T_{c1M} & & & \\ & T_{c2M} & & \\ & & \ddots & \\ & & & T_{cnM} \end{bmatrix}_{2n\times 2n} \tag{6}$$

Next, the reference frame of DG1 is set as the common reference frame. According to the Kirchhoff's voltage law, the following formula will be gotten.

$$\begin{aligned} e_{DQ1} &= (R_{c1}+R_l) i_{DQ1} + (L_{c1}+L_l) \begin{bmatrix} 0 & -\omega_o \\ \omega_o & 0 \end{bmatrix} i_{DQ1} + \\ &(L_{c1}+L_l)\frac{di_{DQ1}}{dt} + R_l i_{DQ2} + L_l \begin{bmatrix} 0 & -\omega_o \\ \omega_o & 0 \end{bmatrix} i_{DQ2} + L_l \frac{di_{DQ2}}{dt} + \\ &\cdots + R_l i_{DQn} + L_l \begin{bmatrix} 0 & -\omega_o \\ \omega_o & 0 \end{bmatrix} i_{DQn} + L_l \frac{di_{DQn}}{dt} \end{aligned} \tag{7}$$

The small signal form of (7) is shown in (8)

$$\left[\Delta e_{DQ}\right] = A_s \left[\Delta i_{DQ}\right] + B_s \left[\Delta \dot{i}_{DQ}\right] \tag{8}$$

(8) can be transformed to

$$\left[\Delta \dot{i}_{DQ}\right] = -B_s^{-1} A_s \left[\Delta i_{DQ}\right] + B_s^{-1} \left[\Delta e_{DQ}\right] \tag{9}$$

Where

$$\left[\Delta e_{DQ}\right]=\left[\Delta e_{DQ1}\quad \Delta e_{DQ2}\quad \cdots\quad \Delta e_{DQn}\right]^T$$

$$\left[\Delta i_{DQ}\right]=\left[\Delta i_{DQ1}\quad \Delta i_{DQ2}\quad \cdots\quad \Delta i_{DQn}\right]^T$$

$A_s=$

$$\begin{bmatrix} R_{c1}+R_l & -\omega_0(L_{c1}+L_l) & R_l & -\omega_0 L_l & \cdots & R_l & -\omega_0 L_l \\ \omega_0(L_{c1}+L_l) & R_{c1}+R_l & \omega_0 L_l & R_l & \cdots & \omega_0 L_l & R_l \\ R_l & -\omega_0 L_l & R_{c2}+R_l & -\omega_0(L_{c2}+L_l) & \cdots & R_l & -\omega_0 L_l \\ \omega_0 L_l & R_l & \omega_0(L_{c2}+L_l) & R_{c2}+R_l & \cdots & \omega_0 L_l & R_l \\ \vdots & \vdots & \vdots & \vdots & \ddots & \vdots & \vdots \\ R_l & -\omega_0 L_l & R_l & -\omega_0 L_l & \cdots & R_{cn}+R_l & -\omega_0(L_{cn}+L_l) \\ \omega_0 L_l & R_l & \omega_0 L_l & R_l & \cdots & \omega_0(L_{cn}+L_l) & R_{cn}+R_l \end{bmatrix}_{2n\times 2n}$$

$$B_s=\begin{bmatrix} L_{c1}+L_l & 0 & L_l & 0 & & L_l & 0 \\ 0 & L_{c1}+L_l & 0 & L_l & \cdots & 0 & L_l \\ L_l & 0 & L_{c2}+L_l & 0 & \cdots & L_l & 0 \\ 0 & L_l & 0 & L_{c2}+L_l & \cdots & 0 & L_l \\ \vdots & \vdots & \vdots & \vdots & \ddots & \vdots & \vdots \\ L_l & 0 & L_l & 0 & \cdots & L_{cn}+L_l & 0 \\ 0 & L_l & 0 & L_l & \cdots & 0 & L_{cn}+L_l \end{bmatrix}_{2n\times 2n} \tag{10}$$

(9) can be transformed to

$$T_1\begin{bmatrix}\Delta\dot{i}_{dq1}\\ \Delta\dot{i}_{dq2}\\ \vdots\\ \Delta\dot{i}_{dqn}\end{bmatrix}+T_2\begin{bmatrix}\Delta\dot{\delta}_{11}\\ \Delta\dot{\delta}_{21}\\ \vdots\\ \Delta\dot{\delta}_{n1}\end{bmatrix}=$$
$$-B_s^{-1}A_sT_1\begin{bmatrix}\Delta i_{dq1}\\ \Delta i_{dq2}\\ \vdots\\ \Delta i_{dqn}\end{bmatrix}+B_s^{-1}T_1\begin{bmatrix}\Delta e_{dq1}\\ \Delta e_{dq2}\\ \vdots\\ \Delta e_{dqn}\end{bmatrix}+(B_s^{-1}T_2-B_s^{-1}A_sT_2)\begin{bmatrix}\Delta\delta_{11}\\ \Delta\delta_{21}\\ \vdots\\ \Delta\delta_{n1}\end{bmatrix} \tag{11}$$

The instantaneous active and reactive power components P and Q are calculated from the measured output voltage and output current as (12).

$$\begin{cases} P_i=1.5\times(e_{id}i_{id}+e_{iq}i_{iq}) \\ Q_i=1.5\times(e_{id}i_{iq}-e_{iq}i_{id}) \end{cases} \tag{12}$$

The active power sharing for different inverters is obtained by introducing droop control as shown in (13) [1]-[5]. Here, e0d stands for the nominal set point of d-axis output voltage and the q-axis reference is set to zero.

$$\begin{cases} \omega=\omega_0-k_{\mathrm{p}}P_{\mathrm{mean}} \\ e_{\mathrm{d}}=e_{0\mathrm{d}}-k_{\mathrm{q}}Q_{\mathrm{mean}} \\ e_{\mathrm{q}}=0 \end{cases} \tag{13}$$

A low pass filter given by (14) is used in order to ensure the control laws defined by (13), ωf is the cut-off frequency of the measuring filter and it is generally chosen to be one-tenth of 50Hz [24].

$$\begin{cases} P_{\mathrm{mean}}=\dfrac{\omega_{\mathrm{f}}}{s+\omega_{\mathrm{f}}}P \\ Q_{\mathrm{mean}}=\dfrac{\omega_{\mathrm{f}}}{s+\omega_{\mathrm{f}}}Q \end{cases} \tag{14}$$

The reference frame of DG1 is taken as the common frame. To translate the variables from an individual inverter reference frame into the common frame, an angle δ is defined for each inverter as shown in (15).

$$\delta_{i1}=\int(\omega_i-\omega_1)dt \tag{15}$$

The small signal equation of (12)-(15) is shown in (16).

$$\begin{cases} \Delta\dot{\delta}_{i1}=\Delta\gamma_i \\ \Delta\dot{\gamma}_i=-k_p\omega_f(\Delta P_i-\Delta P_1)-\omega_f\Delta\gamma_i \end{cases} \tag{16}$$

Where

$$\begin{cases} \Delta P_i=1.5\times(e_{\mathrm{d}i}\Delta i_{\mathrm{d}i}+\Delta e_{\mathrm{d}i}i_{\mathrm{d}i}+e_{\mathrm{q}i}\Delta i_{\mathrm{q}i}+\Delta e_{\mathrm{q}i}i_{\mathrm{q}i}) \\ \Delta Q_i=1.5\times(e_{\mathrm{d}i}\Delta i_{\mathrm{q}i}+\Delta e_{\mathrm{d}i}i_{\mathrm{q}i}-e_{\mathrm{q}i}\Delta i_{\mathrm{d}i}-\Delta e_{\mathrm{q}i}i_{\mathrm{d}i}) \end{cases}$$

When there are n inverters,

$$\begin{bmatrix}\Delta\dot{\gamma}_1\\ \Delta\dot{\gamma}_2\\ \vdots\\ \Delta\dot{\gamma}_n\end{bmatrix}=C_s\left[\Delta i_{dq}\right]+D_s\left[\Delta e_{dq}\right]+F_s\begin{bmatrix}\Delta\gamma_1\\ \Delta\gamma_2\\ \vdots\\ \Delta\gamma_n\end{bmatrix} \tag{17}$$

$$\begin{bmatrix}\Delta\dot{\delta}_{11}\\ \Delta\dot{\delta}_{21}\\ \vdots\\ \Delta\dot{\delta}_{n1}\end{bmatrix}=I_s\begin{bmatrix}\Delta\gamma_1\\ \Delta\gamma_2\\ \vdots\\ \Delta\gamma_n\end{bmatrix} \tag{18}$$

$$\left[\Delta\dot{e}_{dq}\right]=G_s\left[\Delta e_{dq}\right]+H_s\left[\Delta i_{dq}\right] \tag{19}$$

Where *I*s is a unit matrix of n×n order and

$C_s=$

$$\begin{bmatrix} 0 & 0 & 0 & 0 & \cdots & 0 & 0 \\ 1.5k_p\omega_f e_{d1} & 1.5k_p\omega_f e_{q1} & -1.5k_p\omega_f e_{d2} & -1.5k_p\omega_f e_{q2} & \cdots & 0 & 0 \\ \vdots & \vdots & \vdots & \vdots & \ddots & \vdots & \vdots \\ 1.5k_p\omega_f e_{d1} & 1.5k_p\omega_f e_{q1} & 0 & 0 & \cdots & -1.5k_p\omega_f e_{dn} & -1.5k_p\omega_f e_{qn} \end{bmatrix}_{n\times 2n}$$

$D_s=$

$$\begin{bmatrix} 0 & 0 & 0 & 0 & \cdots & 0 & 0 \\ 1.5k_p\omega_f i_{d1} & 1.5k_p\omega_f i_{q1} & -1.5k_p\omega_f i_{d2} & -1.5k_p\omega_f i_{q2} & \cdots & 0 & 0 \\ \vdots & \vdots & \vdots & \vdots & \ddots & \vdots & \vdots \\ 1.5k_p\omega_f i_{d1} & 1.5k_p\omega_f i_{q1} & 0 & 0 & \cdots & -1.5k_p\omega_f i_{d2} & -1.5k_p\omega_f i_{d2} \end{bmatrix}_{n\times 2n}$$

$$F_s=\begin{bmatrix} -\omega_f & & & \\ & -\omega_f & & \\ & & \ddots & \\ & & & -\omega_f \end{bmatrix}_{n\times n}$$

$G_s=$

$$\begin{bmatrix} -\omega_f-1.5k_q\omega_f i_{q1} & 1.5k_q\omega_f i_{d1} & 0 & 0 & \cdots & 0 & 0 \\ 0 & 0 & 0 & 0 & \cdots & 0 & 0 \\ 0 & 0 & -\omega_f-1.5k_q\omega_f i_{q2} & 1.5k_q\omega_f i_{d2} & \cdots & 0 & 0 \\ 0 & 0 & 0 & 0 & \cdots & 0 & 0 \\ \vdots & \vdots & \vdots & \vdots & \ddots & \vdots & \vdots \\ 0 & 0 & 0 & 0 & \cdots & -\omega_f-1.5k_q\omega_f i_{qn} & 1.5k_q\omega_f i_{dn} \\ 0 & 0 & 0 & 0 & \cdots & 0 & 0 \end{bmatrix}_{2n\times 2n}$$

$$H_s = \begin{bmatrix} 1.5k_q\omega_f e_{q1} & -1.5k_q\omega_f e_{d1} & 0 & 0 & \cdots & 0 & 0 \\ 0 & 0 & 0 & 0 & \cdots & 0 & 0 \\ 0 & 0 & 1.5k_q\omega_f e_{q2} & -1.5k_q\omega_f e_{d2} & \cdots & 0 & 0 \\ 0 & 0 & 0 & 0 & \cdots & 0 & 0 \\ \vdots & \vdots & \vdots & \vdots & \ddots & \vdots & \vdots \\ 0 & 0 & 0 & 0 & \cdots & 1.5k_q\omega_f e_{qn} & 0 \\ 0 & 0 & 0 & 0 & \cdots & 0 & -1.5k_q\omega_f e_{dn} \end{bmatrix}_{2n\times 2n}$$

Now, a complete state-space small-signal model of n inverters can be obtained as shown in (20) by combining (11), (17), (18) and (19).

$$\left[\Delta\dot{X}_S\right] = A_{mg\_S}\left[\Delta X_S\right] \tag{20}$$

Where

$$\left[\Delta X_S\right] = \left[\Delta\delta_{11} \quad \Delta\gamma_1 \quad \Delta e_{dq1} \quad \Delta i_{dq1} \quad \Delta\delta_{21} \quad \Delta\gamma_2 \quad \Delta e_{dq2} \quad \Delta i_{dq2} \quad \cdots \quad \Delta\delta_{n1} \quad \Delta\gamma_n \quad \Delta e_{dqn} \quad \Delta i_{dqn}\right]$$

$$A_{mg\_S} = \begin{bmatrix} T_1N_s + T_2J_s \\ K_s \\ J_s \\ M_s \end{bmatrix}^{-1} \begin{bmatrix} B_s^{-1}T_1M_s - B_s^{-1}A_sT_1N_s + B_s^{-1}T_2J_s - B_s^{-1}A_sT_2J_s \\ C_sN_s + D_sM_s + F_sK_s \\ I_sK_s \\ G_sM_s + H_sN_s \end{bmatrix}_{6n\times 6n}$$

$$\begin{bmatrix} \Delta\delta_{11} \\ \Delta\delta_{21} \\ \vdots \\ \Delta\delta_{n1} \end{bmatrix} = [J_s]_{n\times 6n}[\Delta X_s], \quad \begin{bmatrix} \Delta\gamma_1 \\ \Delta\gamma_2 \\ \vdots \\ \Delta\gamma_n \end{bmatrix} = [K_s]_{n\times 6n}[\Delta X_s],$$

$$\begin{bmatrix} \Delta e_{dq1} \\ \Delta e_{dq2} \\ \vdots \\ \Delta e_{dqn} \end{bmatrix} = [M_s]_{2n\times 6n}[\Delta X_s], \quad \begin{bmatrix} \Delta i_{dq1} \\ \Delta i_{dq2} \\ \vdots \\ \Delta i_{dqn} \end{bmatrix} = [N_s]_{2n\times 6n}[\Delta X_s] \tag{21}$$

III. MATH SMALL SIGNAL MODEL OF A MICROGRID WITH STATIC LOADS ACCURACY AND ITS APPLICATION ANALYSIS

A. Small Signal Model Accuracy Analysis of an Autonomous Microgrid with Static Loads

The droop gains influence on low-frequency stability is analyzed and eigenvalue trajectory obtained by proposed model when droop gains change should be compared with that obtained by [11] which had been verified to be accurate enough. A three inverters connected microgrid is studied as an example to calculate the eigenvalues of the system. Noting that the model in [11] describes the complete control loops including voltage loop, current loop and power loop. So the eigenvalues in [11] are composed of three different clusters shown in Fig. 2 where the parameters are presented in table I. From Fig. 2, different clusters eigenvalues indicate the system eigenvalues frequency domain distribution and there is a cluster of low-frequency eigenvalues which are dominant.

TABLE I
INVERTER AND CONTROL PARAMETERS

Components and parameters	Value
DC Voltage. V_{dc}	800v
Switching frequency. f_s	10KHz
Grid frequency. ω	$2\pi\times 50$rad/s
Grid voltage. E_o	311V
LC filter inductor. L_f and R_f	1.35mH, 0.1Ω
LC filter capacitor. C_f	50μF
Line impedance inductor. L_c and R_c	1.8mH, 0.6Ω
Active power droop coefficient. K_p	5×10^{-5}Hz/W
Reactive power droop coefficient. K_q	8.5×10^{-4}V/Var
Cutoff frequency of power calculation LPF.ω_f	$2\pi\times5$rad/s
Voltage loop PI. K_{pv} and K_{iv}	0.05, 390
Current loop PI. K_{pi} and K_{ii}	10.5, 16000

In order to investigate the model accuracy, change the droop coefficients from small to large. Fig. 3(a) depicts the damping of the dominant low-frequency eigenvalues as the active power droop gain increases from 5×10^{-5}Hz/W to 5×10^{-4}Hz/W, where the "*" line represents the eigenvalues in [11] and the "△" line represents the model proposed. Coincident with the conclusion in [11], the eigenvalues of these two models fall into the same area and the eigenvalues move to the right half plane which means the system tends to be unstable when the active power droop gain increases. Similarly, Fig. 3(b) shows the damping of the dominant low-frequency eigenvalues as the reactive power droop gain increases from 8.5×10^{-4}V/Var to 3.9×10^{-3}V/Var, where the red line represents the eigenvalues in [11] and the blue line represents the new model proposed. As it can be seen, the eigenvalues of these two models fall into the same area and both eigenvalues of proposed model and [11] tend to move into the right half plane. In summary, the proposed model and [11] are close matched from the point of the eigenvalues distribution.

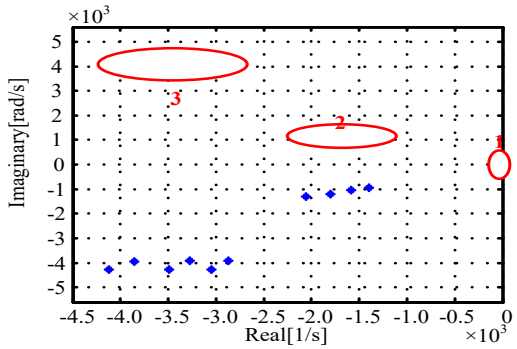

Fig. 2. Overall eigenvalue spectrum of the microgrid system in [11].

Further, one static load is taken into consideration and its parameters are list in Table I. Fig.4 shows the output power of inverters under different conditions of kp. Fig. 4(a) shows the output power of the three inverters when kp is equal to 5×10^{-5}Hz/W and the system keep stable in this case. The performance of microgrid is deteriorated when increasing kp equal to 5×10^{-4}Hz/W and a low-frequency oscillation occurs as shown in Fig. 4(b). The oscillation performance are coincident

with the eigenvalue analysis of the proposed 6n order mathematical model in Fig. 3(a) and it further illustrates that the stability margins are well predicted by the proposed model. Similarly, system tends to be unstable and low-frequency oscillation emerges when kq increases from 8.5×10^{-4}V/Var to 3.9×10^{-3}V/Var. Eigenvalue analysis of the proposed 6n order mathematical model in Fig. 3(b) is shown in Fig. 4(c).

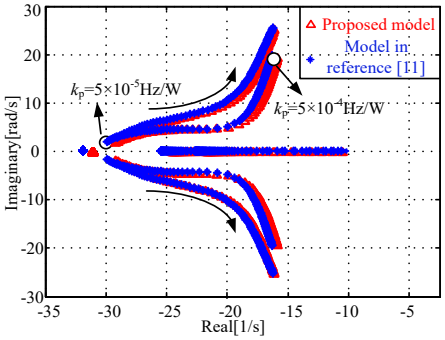

(a) Low-frequency eigenvalue trace of microgrid with RL load when increasing active power droop gain

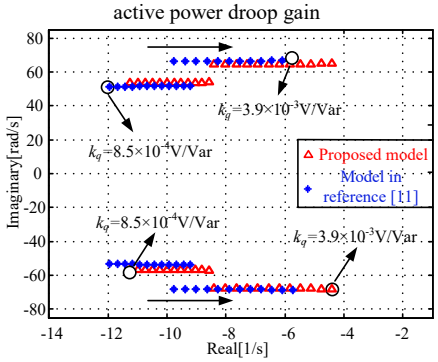

(b) Low-frequency eigenvalue trace of microgrid with RL load when increasing reactive power droop gain

Fig. 3. Damping of the dominant low-frequency mode.

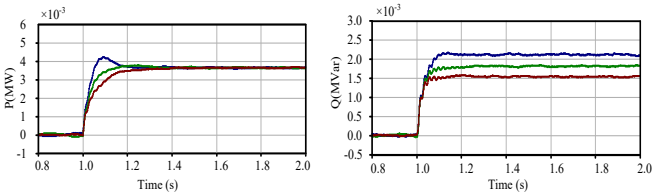

(a) Power of inverters when load increases with small droop gain (5×10-5 Hz/W, 8.5×10-4V/Var).

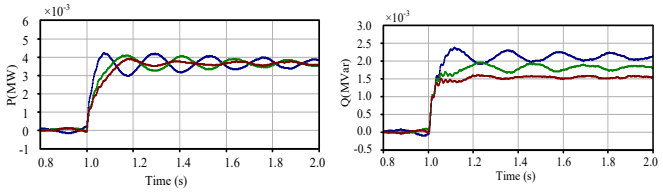

(b) Power of inverters when load increases with large active power droop gain (5×10-4Hz/W, 8.5×10-4V/Var)

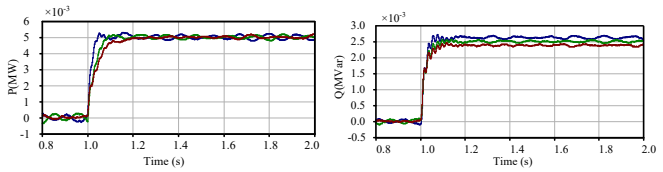

(c) Power of inverters when load increases with large reactive power droop gain (5×10-5 Hz/W, 3.9×10-3V/Var)

Fig. 4. Output power of inverters with static load.

B. Application of the 6n Model of the Autonomous Microgrid with IM Loads connected

By using an IM load in place of the RL load, the relationship between the IM's stator and rotor voltages and currents can be expressed in the synchronous rotating frame by (22)-(25) [13]

$$v_{Ds} = -\omega L_{ss} i_{Qs} + r_s i_{Ds} + L_{ss}\frac{di_{Ds}}{dt} - \omega L_m i_{Qr} + L_m \frac{di_{Dr}}{dt} \tag{22}$$

$$v_{Qs} = \omega L_{ss} i_{Ds} + r_s i_{Qs} + L_{ss}\frac{di_{Qs}}{dt} + \omega L_m i_{Dr} + L_m \frac{di_{Qr}}{dt} \tag{23}$$

$$v_{Dr} = -s\omega L_{rr} i_{Qr} + r_r i_{Dr} + L_{rr}\frac{di_{Dr}}{dt} - s\omega L_m i_{Qs} + L_m \frac{di_{Ds}}{dt} \tag{24}$$

$$v_{Qr} = s\omega L_{rr} i_{Dr} + r_r i_{Qr} + L_{rr}\frac{di_{Qr}}{dt} + s\omega L_m i_{Ds} + L_m \frac{di_{Qs}}{dt} \tag{25}$$

Where L_{ss} and r_s are the stator inductance and resistance, L_{rr} and r_r are the corresponding rotor parameters, Lm, s and ω are the linkage inductance, rotor slip, and the stator supply angular frequency respectively.

Besides, the relationship between torque and the mechanical speed can be derived in terms of the motor slip and stator angular speed as follows

$$\begin{aligned} T_L &= T_e - J\frac{d((1-s)\omega)}{dt} \\ &= \frac{3}{4}\rho L_m(i_{Qs}i_{Dr} - i_{Ds}i_{Qr}) - J\frac{d((1-s)\omega)}{dt} \end{aligned} \tag{26}$$

In (26), T_e is the electromagnetic torque, ρ, J and T_L are the number of poles, combined motor and load inertia, and the load torque respectively.

According to the Kirchhoff's voltage law and setting the reference frame of IM load as common reference frame, we can get the following formula

$$\begin{aligned} e_{Di} &= R_{ci} i_{Di} + L_{ci}\frac{di_{Di}}{dt} - \omega L_{ci} i_{Qi} + v_{Ds} \\ e_{Qi} &= R_{ci} i_{Qi} + L_{ci}\frac{di_{Qi}}{dt} + \omega L_{ci} i_{Di} + v_{Qs} \end{aligned} \tag{27}$$

Where i (n=1, 2.....k) represents the number of inverters. (28) can be obtained by combining (24), (25), (26) and (27).

$$\begin{aligned} \left[\Delta e_{DQ\_IM}\right] &= A_{IM}\left[\Delta i_{DQ\_IM}\right] + B_{IM}[\Delta i_{DQs}] + C_{IM}\begin{bmatrix}\Delta i_{DQr}\\ \Delta s\end{bmatrix} \\ &+ D_{IM}\left[\Delta \dot{i}_{DQ\_IM}\right] F_{IM}[\Delta \dot{i}_{DQs}] + G_{IM}\begin{bmatrix}\Delta \dot{i}_{DQr}\\ \Delta \dot{s}\end{bmatrix} \\ &= (A_{IM} + B_{IM}S_{IM})\left[\Delta i_{DQ\_IM}\right] + C_{IM}\begin{bmatrix}\Delta i_{DQr}\\ \Delta s\end{bmatrix} \\ &+ (D_{IM} + F_{IM}S_{IM})\left[\Delta \dot{i}_{DQ\_IM}\right] + G_{IM}\begin{bmatrix}\Delta \dot{i}_{DQr}\\ \Delta \dot{s}\end{bmatrix} \end{aligned} \tag{28}$$

Where

$$\begin{aligned} \left[\Delta e_{DQ\_IM}\right] &= \left[\Delta e_{DQ1} \quad \Delta e_{DQ2} \quad \cdots \quad \Delta e_{DQn}\right]^T \\ \left[\Delta i_{DQ\_IM}\right] &= \left[\Delta i_{DQ1} \quad \Delta i_{DQ2} \quad \cdots \quad \Delta i_{DQn}\right]^T \end{aligned} \tag{29}$$

The other matrices in (28) are given in Appendix. (30) can be obtained according to (5).

$$\begin{aligned}&(D_{IM}+F_{IM}S_{IM})T_1\left[\Delta\dot{i}_{dq\_IM}\right]+(D_{IM}+F_{IM}S_{IM})T_2\begin{bmatrix}\Delta\dot{\delta}_{1IM}\\ \Delta\dot{\delta}_{2IM}\\ \vdots\\ \Delta\dot{\delta}_{nIM}\end{bmatrix}+G_{IM}\begin{bmatrix}\Delta\dot{i}_{DQr}\\ \Delta\dot{s}\end{bmatrix}\\ &=T_1\left[\Delta e_{dq\_IM}\right]-(A_{IM}+B_{IM}S_{IM})T_1\left[\Delta i_{dq\_IM}\right]+\\ &(A_{IM}+B_{IM}S_{IM})T_2\begin{bmatrix}\Delta\delta_{1IM}\\ \Delta\delta_{2IM}\\ \vdots\\ \Delta\delta_{nIM}\end{bmatrix}-C_{IM}\begin{bmatrix}\Delta i_{DQr}\\ \Delta s\end{bmatrix}\end{aligned}\tag{30}$$

According to (24) and (25), (31) and (32) can be obtained.

$$\begin{bmatrix}\Delta v_{DQr}\\ \Delta T_L\end{bmatrix}=H_{IM}\left[\Delta i_{DQ\_IM}\right]+J_{IM}\begin{bmatrix}\Delta i_{DQr}\\ \Delta s\end{bmatrix}+K_{IM}\left[\Delta\dot{i}_{DQ\_IM}\right]+M_{IM}\begin{bmatrix}\Delta\dot{i}_{DQr}\\ \Delta\dot{s}\end{bmatrix}\tag{31}$$

$$\begin{aligned}&K_{IM}S_{IM}T_1\left[\Delta\dot{i}_{dq\_IM}\right]+K_{IM}S_{IM}T_2\begin{bmatrix}\Delta\dot{\delta}_{1IM}\\ \Delta\dot{\delta}_{2IM}\\ \vdots\\ \Delta\dot{\delta}_{nIM}\end{bmatrix}+M_{IM}\begin{bmatrix}\Delta\dot{i}_{DQr}\\ \Delta\dot{s}\end{bmatrix}\\ &=\begin{bmatrix}\Delta v_{DQr}\\ \Delta T_L\end{bmatrix}-H_{IM}S_{IM}T_1\left[\Delta i_{dq\_IM}\right]-H_{IM}S_{IM}T_2\begin{bmatrix}\Delta\delta_{1IM}\\ \Delta\delta_{2IM}\\ \vdots\\ \Delta\delta_{nIM}\end{bmatrix}-J_{IM}\begin{bmatrix}\Delta i_{DQr}\\ \Delta s\end{bmatrix}\end{aligned}\tag{32}$$

The matrices in (31) and (32) are given in Appendix. And next is power loop which is similar with before.

$$\begin{bmatrix}\Delta\dot{\gamma}_1\\ \Delta\dot{\gamma}_2\\ \vdots\\ \Delta\dot{\gamma}_n\end{bmatrix}=O_{IM}\left[\Delta i_{dq\_IM}\right]+P_{IM}\left[\Delta e_{dq\_IM}\right]+Q_{IM}\begin{bmatrix}\Delta\gamma_1\\ \Delta\gamma_2\\ \vdots\\ \Delta\gamma_n\end{bmatrix}\tag{33}$$

$$\begin{bmatrix}\Delta\dot{\delta}_{1IM}\\ \Delta\dot{\delta}_{2IM}\\ \vdots\\ \Delta\dot{\delta}_{nIM}\end{bmatrix}=I_{IM}\begin{bmatrix}\Delta\gamma_1\\ \Delta\gamma_2\\ \vdots\\ \Delta\gamma_n\end{bmatrix}\tag{34}$$

$$\left[\Delta\dot{e}_{dq\_IM}\right]=U_{IM}\left[\Delta e_{dq\_IM}\right]+V_{IM}\left[\Delta i_{dq\_IM}\right]\tag{35}$$

Where IIM is a unit matrix of n×n-order and the other matrices in (33) (34) and (35) are given in Appendix.

Now, a state-space small-signal model of n inverters with IM load shown in (36) can be obtained by combining (30), (31), (32) and (33).

$$\left[\Delta\dot{X}_{IM}\right]=A_{mg\_IM}\left[\Delta X_{IM}\right]\tag{36}$$

Where

$$\begin{aligned}\left[\Delta X_{IM}\right]=\big[&\Delta\delta_{1IM}\quad\Delta\gamma_1\quad\Delta e_{dq1}\quad\Delta i_{dq1}\quad\Delta\delta_{2IM}\quad\Delta\gamma_2\quad\Delta e_{dq2}\\ &\Delta i_{dq2}\quad\cdots\quad\Delta\delta_{nIM}\quad\Delta\gamma_n\quad\Delta e_{dqn}\quad\Delta i_{dqn}\quad\Delta i_{DQr}\quad\Delta s\big]\end{aligned}\tag{37}$$

$$A_{mg\_IM}=\begin{bmatrix}(D_{IM}+F_{IM}S_{IM})(T_1Z_{IM}+T_2W_{IM})+G_{IM}R_{IM}\\ K_{IM}S_{IM}T_1Z_{IM}+K_{IM}S_{IM}T_2W_{IM}+M_{IM}R_{IM}\\ X_{IM}\\ W_{IM}\\ Y_{IM}\end{bmatrix}^{-1}\times\begin{bmatrix}T_1Y_{IM}-(A_{IM}+B_{IM}S_{IM})T_1Z_{IM}+(A_{IM}+B_{IM}S_{IM})T_2W_{IM}-C_{IM}R_{IM}\\ -H_{IM}S_{IM}T_1Z_{IM}-H_{IM}S_{IM}T_2W_{IM}-J_{IM}R_{IM}\\ O_{IM}Z_{IM}+P_{IM}Y_{IM}+Q_{IM}X_{IM}\\ I_{IM}X_{IM}\\ U_{IM}Y_{IM}+V_{IM}Z_{IM}\end{bmatrix}_{(6n+3)\times(6n+3)}\tag{38}$$

The matrices in $A_{\mathrm{mg\_IM}}$ are given in Appendix.

In order to demonstrate the accuracy of the 6n-order model of the autonomous microgrid with IM load, the eigenvalue trajectory of a complete model in [13] is plotted in Fig. 5. According to the matrix in (38), Fig. 5 shows the relationship between eigenvalue trajectory and active power droop gain k_p when it increases from 3×10^{-5}Hz/W to 15×10^{-5}Hz/W. The other parameters of IM load are shown in Table II. From Fig. 5 it can be observed that the dominant eigenvalue trajectory tends to the right half-plane when the active power droop gain increases. In the proposed model, the critical point of the system is k_p = 15×10^{-5}Hz/W in the proposed model and in [13] k_p = 14.3×10^{-5}Hz/W. This is very close and the proposed model can be used to predict the stability of the system. Due to induction motor load, the eigenvalue trajectory is quite different from that of microgrid with static load. The eigenvalues tend to the right half-plane which indicates that low-frequency oscillation will occur. But when the equivalent IM load is connected, even under the same droop gains, the eigenvalues show much less damped behavior than the eigenvalues of microgrid with static load.

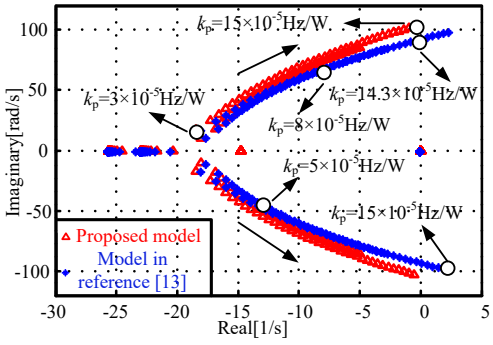

Fig. 5. Low-frequency eigenvalue trace of microgrid with IM load when increasing the active power droop gain.

Fig. 6(a) shows the power of inverters when the equivalent IM load is connected and *k*p is equal to 5×10^{-5}Hz/W at this moment. Fig. 6(a) shows much less damped behavior than Fig. 4(a) even under the same *k*p. And this is coincident with previous conclusion in Fig. 5 and Part III B. The influence of active power gain *k*p on the system stability is show in Fig. 6(b) which shows the motor speed response with different *k*p. It should be noted that the system yields to low-frequency oscillation with the increasing of active power droop gain from 5×10^{-5}Hz/W to 8×10^{-5}Hz/W and this coincides with Fig. 5 and Part III B. The parameters of IM load is shown in Table II.

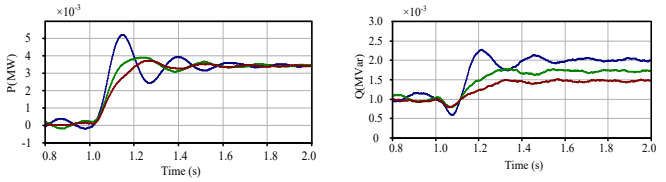

(a) Power of inverters when equivalent IM load is connected with small active power droop gain (5×10-5Hz/W, 8.5×10-4V/Var).

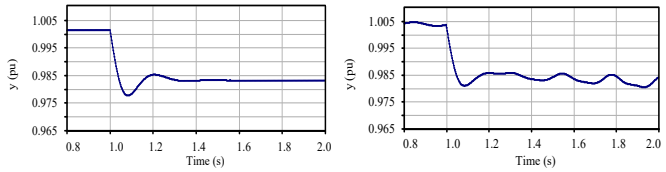

(b) Motor speed response when equivalent IM load is connected from small active power droop gain (5×10-5Hz/W) to large active power droop gain (8×10-5Hz/W).

Fig. 6. Output power of inverters with IM load.

TABLE II
IM LOAD PARAMETERS

Components and parameters	Value
Linkage inductance, L_m	193mH
Rotor inductance and resistance. L_{rr} and r_r	207mH, 3.433Ω
Stator inductance and resistance. L_{ss} and r_s	203mH, 5.533Ω
Inertia. J	0.008Kg·m²
Number of poles. P	4

C. Application of the 6n-oder Model of the Autonomous Microgrid with CP Loads

DC loads are connected to microgrid through controllable or uncontrollable rectifiers and consume constant power which have negative incremental impedance characteristic, as this reason it can be classified as CP loads.

As mentioned in [25], there is a small perturbation in voltage and current as shown in the following equation.

$$\frac{\tilde{V}}{\tilde{I}} = -\frac{V}{I} = -\left|Z_{CPL}\right| \tag{39}$$

Where V and I are the peak voltage and peak current. -|ZCPL| can be obtained by the following calculation:

$$\left|Z_{CPL}\right| = \frac{V}{I} = \frac{V_r}{I_r} = \frac{V_r^2}{P}\cos\alpha \tag{40}$$

Where Vr, Ir are RMS values. α is the phase difference. Finally, the equivalent resistance R_{CPL} and inductance L_{CPL} can be calculated by this form.

$$\begin{cases} R_{CPL} = -\left|Z_{CPL}\right|\cos\alpha \\ L_{CPL} = -\dfrac{\left|Z_{CPL}\right|\cos\alpha}{\omega} \end{cases} \tag{41}$$

In summary, the difference between model of microgrid with CP load and model proposed in Section III is that the load is negative impedance characteristic. For simplicity, the state-space small-signal model of the n inverters with CP load can be obtained according to the proposed method as follows.

$$\left[\Delta\dot{X}_{CP}\right] = A_{mg\_CP}\left[\Delta X_{CP}\right] \tag{42}$$

Where

$$\left[\Delta X_{CP}\right] = \left[\Delta\delta_{1CP} \quad \Delta\gamma_1 \quad \Delta e_{dq1} \quad \Delta i_{dq1} \quad \Delta\delta_{2CP} \quad \Delta\gamma_2 \quad \Delta e_{dq1} \quad \Delta i_{dq1} \quad \cdots \quad \Delta\delta_{nCP} \quad \Delta\gamma_n \quad \Delta e_{dqn} \quad \Delta i_{dqn}\right] \tag{43}$$

$$A_{mg\_CP} = \begin{bmatrix} T_1N_{CP} + T_2J_{CP} \\ K_{CP} \\ J_{CP} \\ M_{CP} \end{bmatrix}^{-1} \begin{bmatrix} B_{CP}^{-1}T_1M_{CP} - B_{CP}^{-1}A_{CP}T_1N_{CP} + B_{CP}^{-1}T_2J_{CP} - B_{CP}^{-1}A_{CP}T_2J_{CP} \\ C_{CP}N_{CP} + D_{CP}M_{CP} + F_{CP}K_{CP} \\ I_{CP}K_{CP} \\ G_{CP}M_{CP} + H_{CP}N_{CP} \end{bmatrix}_{6n\times 6n} \tag{44}$$

The matrices in A_{mg_CP} are equal to the corresponding matrices in A_{mg_S}.

Similarly, Fig. 7 indicates the eigenvalue trajectory of 6n-oder autonomous microgrid model with a CP load marked by "△" line and complete microgrid model with a CP load in [25] marked by "*" line when the active power droop gain increases from 1.57×10^{-5}Hz/W to 3.14×10^{-4}Hz/W. The parameters of CP load are shown in Table III. As can be seen, the eigenvalues of these two models fall into the same area and both eigenvalue trajectories tend to right half-plane and low-frequency oscillation will appear where the oscillation frequency is around 1Hz-15Hz. As it can be seen from Fig. 7, these two trajectories are very close. The error between them should be researched further and this does not affect the stability analysis.

TABLE III
CP LOAD PARAMETERS

Components and parameters	Value
Voltage loop PI. K_{vp} and K_{vi}	0.4, 10
Current loop PI. K_{cp} and K_{ci}	46, 0.5
Filter inductance. L_g	0.7mH
Filter resistance. L_g	0.05Ω
DC-link capacitance. C_{DC}	300uF
DC-link voltage. U_{DC}	700V

Fig. 8(a) and Fig. 8(b) shows the active power of the inverters when the CP load is connected in place of the RL load. The reactive power is zero due to the introduction of CP load and it can be ignored. In Fig. 8(a), system reaches stability fast and kp is equal to 1.57×10^{-5}Hz/W at this moment. However, when the droop gain kp increases from 1.57×10^{-5}Hz/W to 1.6×10^{-4}Hz/W, the low-frequency oscillation phenomenon is more serious shown in Fig. 8(b). The simulation results are identical with Fig. 7and Part III C.

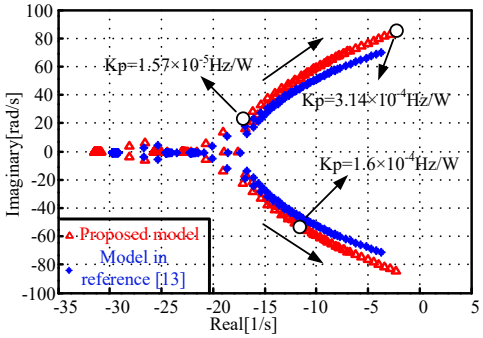

Fig. 7. Low-frequency eigenvalue trace of microgrid with CP load when the active power droop gain increases.

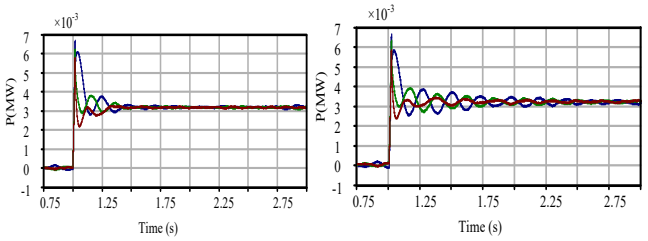

Fig. 8. Output power of inverters with CP load.

(a) Active power of inverters when CP load increases with small active power droop gain (1.57×10^{-5}Hz/W, 8.5×10^{-4}V/Var).

(b) Active power of inverters when CP load increases with large active power droop gain (1.6×10^{-4}Hz/W, 8.5×10^{-4}V/Var)..

IV. Experimental Verification Of Proposed Model

A. Experimental Results with RL Loads

An experimental platform is built to validate the proposed analysis, it consists of two paralleled three-phase inverters. The inverters operate as droop-controlled sources and itse phase voltage is 110Vrms. A resistive–inductive load is connected to PCC. The system parameters are shown as follows: 3KVA, C_{dc}=470uF, L_f=3mH, C_f=14.1uF, f_s=10kHz, ω_f=31.4rad/s, k_{pv}=0.01414, k_{iv}=150, k_{pi}=0.5, k_{ii}=1000, Z_{line1}=1Ω+j0.45mH, Z_{line2}=2Ω+j0.9mH, Z_{load}=50Ω+j7mH.

First of all, a reduced 12 order low-frequency mathematical model of experimental platform is acquired by using the method shown in Section III. Fig. 9 shows the eigenvalue trajectory of the system which are close to the imaginary axis as a function of active power droop gain *k*p and reactive power droop gain *k*q. In Fig. 9(a), the kp increases from 2×10^{-3}Hz/W to 8×10^{-3}Hz/W. The root locus tends to the right-half-plane with the increasing of kp and low-frequency oscillation will appear. Similarly, in Fig. 9(b), the k_q increases from 0.015V/Var to 0.08V/Var. And the eigenvalue trajectory tends to the left side of the complex plane. Fig. 10 shows the active and reactive power and the they are stable and the k_p is equal to 2×10^{-3}Hz/W in this case. When k_p is 8×10^{-3}Hz/W, the system is unstable and the low-frequency oscillation appears in both active power and reactive power shown in Fig. 11(a), (b). And when *k*q increases from 0.015V/Var to 0.08V/Var, the low-frequency oscillation also occurs shown in Fig. 11(c), (d). Therefore, the system stability is degraded when kp or kq increases and this experimental results are coincide with the conclusion of eigenvalue trajectory.

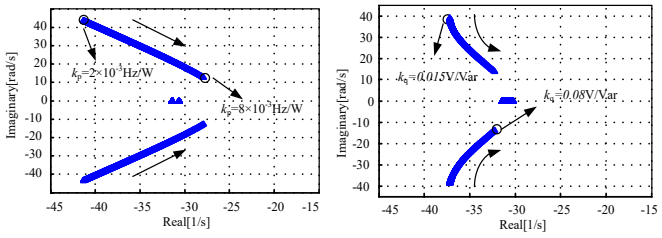

Fig. 9. Eigenvalue trajectory of reduced 12 order model with RL load.

(a) Increasing real power droop gain
(b) Increasing reactive power droop gain

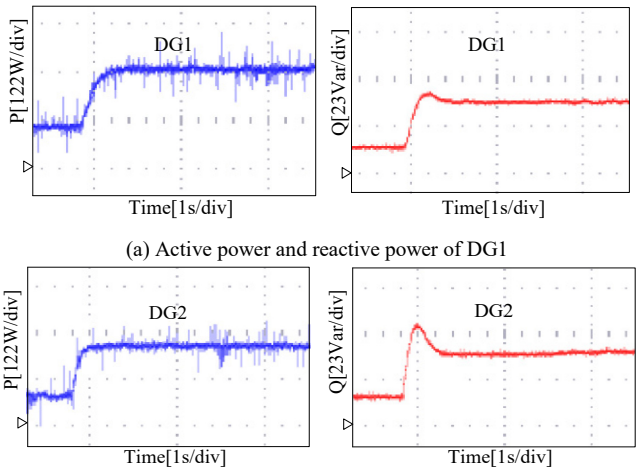

Fig. 10. Power of inverters when load increases with small droop gain (2×10^{-3}Hz/W, 0.015V/var).

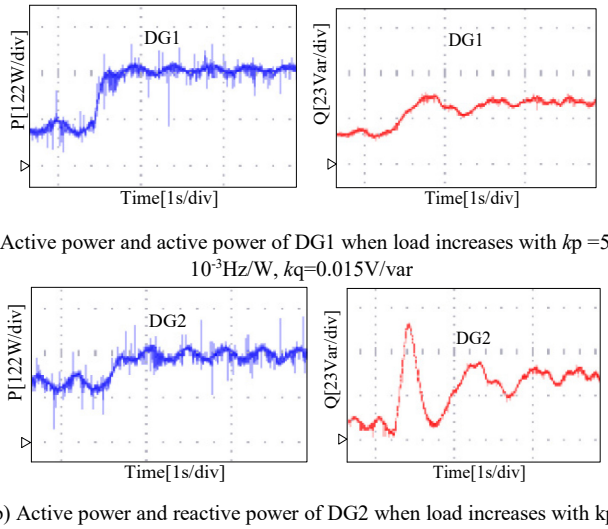

Fig. 11. Output power of inverters when load increases with large droop gain.

B. Experimental Results with IM Loads

The parameter of IM load is listed below. P_N=100W, U_N=220V, I_N=0.48A, n_N=1420rpm, ρ=4. First of all, a reduced

15-order low-frequency mathematical model of experimental platform is obtained according to Section III B. Fig. 12 also shows the eigenvalue trajectory of the system which are close to the imaginary axis when k_p increases from $3\times10^{-}$4Hz/W to 3×10^{-3}Hz/W and the system tends to the left side of the complex plane. It should be noted that the system will be more unstable when k_p is 1.5×10^{-3}Hz/W than k_p is 5×10^{-4}Hz/W. Then the eigenvalue trajectory analysis above will be verified by the experimental results. Fig.13 shows the power of DG1 and DG2. Among them, Fig. 13(a) (b) shows the power when kp is 5×10^{-4}Hz/W and Fig. 13(c) (d) shows the power when k_p is 1.5×10^{-3}Hz/W. The last is more unstable than the former, so this is coincide with the eigenvalue analysis above.

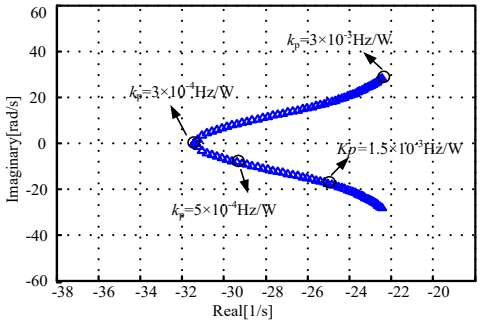

Fig. 12. Eigenvalues trajectory of reduced 15 order model with IM load.

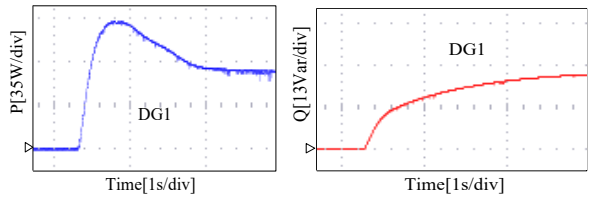

(a) Active power and reactive power of DG1 with small active power droop gain (kp =5×10^{-4}Hz/W, kq=0.075V/var)

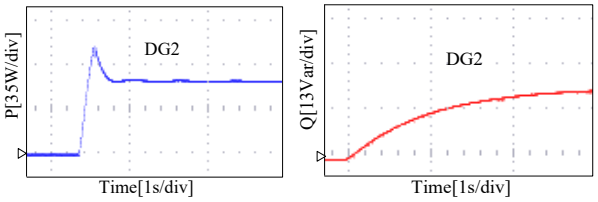

(b) Active power and reactive power of DG2 with small active power droop gain (kp =5×10^{-4}Hz/W, kq=0.075V/var)

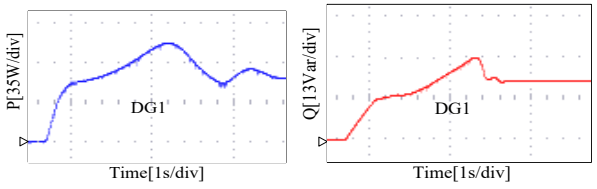

(c) Active power and reactive power of DG1 with large active power droop gain (kp =1.5×10^{-3}Hz/W, kq=0.075V/var)

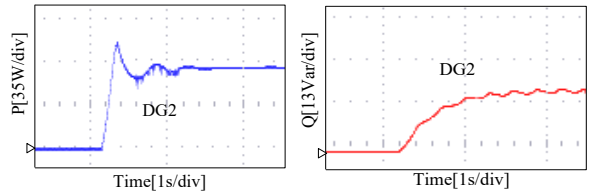

(d) Active power and reactive power of DG2 with large active power droop gain (kp =1.5×10^{-3}Hz/W, kq=0.075V/var)

Fig. 13. Power of inverters when IM load joins.

C. Experimental Results with CP Loads

Because of the limitation of experimental conditions, there are just two inverters in experimental platform. One of them is treated as inverter and the other one is treated as rectifier load. The parameter of rectifier is as follows: Lc=0.45mH, C_f=14.1uF, L_f=3mH, C_{DC}=470uF, U_{DC}=300, R_{LOAD}=150Ω. A reduced 10 order low-frequency mathematical is built according to Section III C. Fig. 14(a) also shows the eigenvalue trajectory which are close to the imaginary axis with the increasing of k_p from 1×10^{-4}Hz/W to 9×10^{-4}Hz/W and the system tends to the left side of the complex plane. Remarkably, the system is more stable when k_p is 5.275×10^{-4}Hz/W than k_p is 8.275×10^{-4}Hz/W. The experimental results are shown in Fig. 14(b),(c). The system is stable when k_p is 5.275×10-4Hz/W while the system tends to be unstable when k_p increases to 8.275×10^{-4}Hz/W. In summary, the experimental results are also coincided with the eigenvalue analysis above.

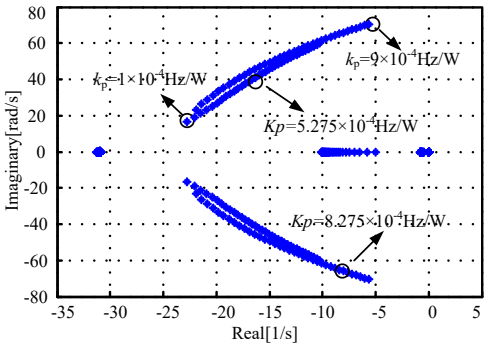

(a)

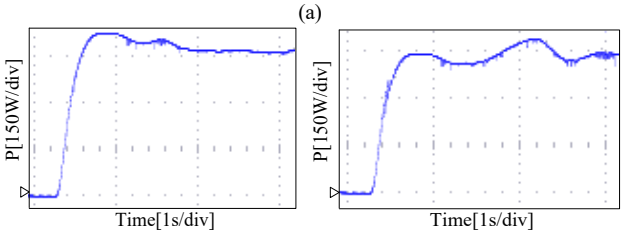

(b) (c)

Fig. 14. Eigenvalues trajectory and power of inverters when CP load joins in.
(a) Eigenvalues trajectory of reduced 10 order model with CP load.
(b) Active power with kp =5.275×10-4Hz/W, kq=0.075V/var
(c) Active power with kp=8.275×10-4Hz/W, kq=0.075V/var

V. Conclusion

In this paper, a novel reduced order low-frequency model for inverter-based microgrid with different loads is proposed. Comparing the 6n-order low-frequency model of microgrid with static load with the complete model, the proposed model which is simpler but also has the same accuracy and reliability for the research of low-frequency stability of the microgrid system. In addition, a 6n+3 and 6n low-frequency small-signal state-space models of a microgrid with induction motor load and constant power load are developed in this paper. Through the eigenvalue trajectory analysis of the proposed model, these kinds of load can also cause the system to produce low-frequency oscillation. Detailed eigenvalue analysis, simulation, and experiment results have been presented to certify the effectiveness of the proposed model.

APPENDIX

$$A_{IM}=\begin{bmatrix} R_{c1} & -\omega L_{c1} & \cdots & 0 & 0 \\ \omega L_{c1} & R_{c1} & \cdots & 0 & 0 \\ \vdots & \vdots & \ddots & \vdots & \vdots \\ 0 & 0 & \cdots & R_{cn} & -\omega L_{cn} \\ 0 & 0 & \cdots & \omega L_{cn} & R_{cn} \end{bmatrix}_{2n\times 2n} \tag{A1}$$

$$B_{IM}=\begin{bmatrix} r_s & -\omega L_{ss} \\ \omega L_{ss} & r_s \\ \vdots & \vdots \\ r_s & -\omega L_{ss} \\ \omega L_{ss} & r_s \end{bmatrix}_{2n\times 2} \tag{A2}$$

$$C_{IM}=\begin{bmatrix} 0 & -\omega L_m & 0 \\ -\omega L_m & 0 & 0 \\ \vdots & \vdots & \vdots \\ 0 & -\omega L_m & 0 \\ -\omega L_m & 0 & 0 \end{bmatrix}_{2n\times 3} \tag{A3}$$

$$D_{IM}=\begin{bmatrix} L_{l1} & & & & \\ & L_{l1} & & & \\ & & \ddots & & \\ & & & L_{ln} & \\ & & & & L_{ln} \end{bmatrix}_{2n\times 2n} \tag{A4}$$

$$F_{IM}=\begin{bmatrix} L_{ss} & 0 \\ 0 & L_{ss} \\ \vdots & \vdots \\ L_{ss} & 0 \\ 0 & L_{ss} \end{bmatrix}_{2n\times 2} \tag{A5}$$

$$G_{IM}=\begin{bmatrix} L_{ss} & 0 & 0 \\ 0 & L_{ss} & 0 \\ \vdots & \vdots & \vdots \\ L_{ss} & 0 & 0 \\ 0 & L_{ss} & 0 \end{bmatrix}_{2n\times 3} \tag{A6}$$

$$S_{IM}=\begin{bmatrix} 1 & 0 & \cdots & \cdots & 1 & 0 \\ 0 & 1 & \cdots & \cdots & 0 & 1 \end{bmatrix}_{2\times 2n} \tag{A7}$$

$$H_{IM}=\begin{bmatrix} 0 & -s\omega L_m \\ s\omega L_m & 0 \\ -\frac{3}{4}\rho L_m i_{Qr} & \frac{3}{4}\rho L_m i_{Dr} \end{bmatrix}_{3\times 2} \tag{A8}$$

$$J_{IM}=\begin{bmatrix} r_r & -s\omega L_{rr} & 0 \\ s\omega L_{rr} & r_r & 0 \\ \frac{3}{4}\rho L_m i_{Qs} & -\frac{3}{4}\rho L_m i_{Qs} & 0 \end{bmatrix}_{3\times 3} \tag{A9}$$

$$K_{IM}=\begin{bmatrix} L_m & 0 \\ 0 & L_m \\ 0 & 0 \end{bmatrix}_{3\times 2} \tag{A10}$$

$$M_{IM}=\begin{bmatrix} L_{ss} & & \\ & L_{ss} & \\ & & J\times\omega_0 \end{bmatrix}_{3\times 3} \tag{A11}$$

$$O_{IM}=\begin{bmatrix} 0 & 0 & 0 & 0 & \cdots & 0 & 0 \\ 1.5k_p\omega_f e_{d1} & 1.5k_p\omega_f e_{q1} & -1.5k_p\omega_f e_{d2} & -1.5k_p\omega_f e_{q2} & \cdots & 0 & 0 \\ \vdots & \vdots & \vdots & \vdots & \ddots & \vdots & \vdots \\ 1.5k_p\omega_f e_{d1} & 1.5k_p\omega_f e_{q1} & 0 & 0 & \cdots & -1.5k_p\omega_f e_{dn} & -1.5k_p\omega_f e_{qn} \end{bmatrix}_{n\times 2n} \tag{A12}$$

$$P_{IM}=\begin{bmatrix} 0 & 0 & 0 & 0 & \cdots & 0 & 0 \\ 1.5k_p\omega_f i_{d1} & 1.5k_p\omega_f i_{q1} & -1.5k_p\omega_f i_{d2} & -1.5k_p\omega_f i_{q2} & \cdots & 0 & 0 \\ \vdots & \vdots & \vdots & \vdots & \ddots & \vdots & \vdots \\ 1.5k_p\omega_f i_{d1} & 1.5k_p\omega_f i_{q1} & 0 & 0 & \cdots & -1.5k_p\omega_f i_{d2} & -1.5k_p\omega_f i_{d2} \end{bmatrix}_{n\times 2n} \tag{A13}$$

$$Q_{IM}=\begin{bmatrix} -\omega_f & & & \\ & -\omega_f & & \\ & & \ddots & \\ & & & -\omega_f \end{bmatrix}_{n\times n} \tag{A14}$$

$$U_{IM}=\begin{bmatrix} -\omega_f-1.5k_q\omega_f i_{q1} & 1.5k_q\omega_f i_{d1} & 0 & 0 & \cdots & 0 & 0 \\ 0 & 0 & 0 & 0 & \cdots & 0 & 0 \\ 0 & 0 & -\omega_f-1.5k_q\omega_f i_{q2} & 1.5k_q\omega_f i_{d2} & \cdots & 0 & 0 \\ 0 & 0 & 0 & 0 & \cdots & 0 & 0 \\ \vdots & \vdots & \vdots & \vdots & \ddots & \vdots & \vdots \\ 0 & 0 & 0 & 0 & \cdots & -\omega_f-1.5k_q\omega_f i_{qn} & 1.5k_q\omega_f i_{dn} \\ 0 & 0 & 0 & 0 & \cdots & 0 & 0 \end{bmatrix}_{2n\times 2n} \tag{A15}$$

$$V_{IM}=\begin{bmatrix} 1.5k_q\omega_f e_{q1} & -1.5k_q\omega_f e_{d1} & 0 & 0 & \cdots & 0 & 0 \\ 0 & 0 & 0 & 0 & \cdots & 0 & 0 \\ 0 & 0 & 1.5k_q\omega_f e_{q2} & -1.5k_q\omega_f e_{d2} & \cdots & 0 & 0 \\ 0 & 0 & 0 & 0 & \cdots & 0 & 0 \\ \vdots & \vdots & \vdots & \vdots & \ddots & \vdots & \vdots \\ 0 & 0 & 0 & 0 & \cdots & 1.5k_q\omega_f e_{qn} & 0 \\ 0 & 0 & 0 & 0 & \cdots & 0 & -1.5k_q\omega_f e_{dn} \end{bmatrix}_{2n\times 2n} \tag{A16}$$

$$\begin{bmatrix} \Delta\delta_{1IM} \\ \Delta\delta_{2IM} \\ \vdots \\ \Delta\delta_{nIM} \end{bmatrix}=[W_{IM}]_{n\times(6n+3)}[\Delta X_{IM}] \tag{A17}$$

$$\begin{bmatrix} \Delta\gamma_1 \\ \Delta\gamma_2 \\ \vdots \\ \Delta\gamma_n \end{bmatrix}=[X_{IM}]_{n\times(6n+3)}[\Delta X_{IM}] \tag{A18}$$

$$\left[\Delta e_{dq\_IM}\right]=[Y_{IM}]_{2n\times(6n+3)}[\Delta X_{IM}] \tag{A19}$$

$$\left[\Delta i_{dq\_IM}\right]=[Z_{IM}]_{2n\times(6n+3)}[\Delta X_{IM}] \tag{A20}$$

$$\begin{bmatrix} \Delta i_{DQr} \\ \Delta s \end{bmatrix}=[R_{IM}]_{3\times(6n+3)}[\Delta X_{IM}] \tag{A21}$$

REFERENCES

[1] A. Chaouachi, R. M. Kamel, R. Andoulsi, and K. Nagasaka, "Multiobjective intelligent energy management for a microgrid," *IEEE Trans. Ind. Electron.*, vol. 60, no. 4, pp. 1688–1699, Apr. 2013.

[2] Rocabert J, Luna A, Blaabjerg F, et al. "Control of Power Converters in AC Microgrids". *IEEE Transactions on Power Electronics*, 2012, vol. 27, no. 11, pp. 4734-4749.

[3] J. M. Guerrero, J. Vasquez, J. Matas, L. D. Vicuna, and M. Castilla, "Hierarchical control of droop-controlled ac and dc Microgrid—a general approach toward standardization," *IEEE Trans. Ind. Electron*., vol. 58, no. 1, pp. 158–172, Jan. 2011.

[4] I. J. Balaguer, Q. Lei, S.Yang, U. Supatti, and F. Z. Peng, "Control for grid connected and intentional islanding operation of distributed power generation," *IEEE Trans. Ind. Electron.*, vol. 58, no. 1, pp. 147–157, Jan. 2011.

[5] T. L. Vandoorn, J. D. M. De Kooning, B. Meersman, J. M. Guerrero, and L. Vandevelde, "Voltage-based control of a smart transformer in a microgrid," *IEEE Trans. Ind. Electron*., vol. 60, no. 4, pp. 1291–1305, Apr. 2013.

[6] A. Radwan and Y.-R. Mohamed, "Analysis and active-impedance-based stabilization of voltage-source-rectifier loads in grid-connected and isolated microgrid applications," *IEEE Trans. Sustain. Energy.,* vol. 4, no. 3, pp. 563–576, Jul. 2013.

[7] X. Wang, F. Blaabjerg, and Z. Chen, "An improved virtual impedance for droop-controlled parallel three-phase voltage source inverters," in *Proc. IEEE ECCE 2012,* in press, 2012.

[8] J. Kwon, X. Wang, and F. Blaabjerg, "Impedance Based Analysis and Design of Harmonic Resonant Controller for a Wide Range of Grid Impedance," *in Proc. 5th Annu. IEEE PEDG* '2014.

[9] J. Sun, "Impedance-based stability criterion for grid-connected inverters," *IEEE Trans. Power Electron.*, vol. 26, no. 11, pp.3075–3078, Nov. 2011.

[10] X. Guo, Z. Lu, B. Wang, X. Sun, L. Wang, and J. M. Guerrero, "Dynamic phasors-based modeling and stability analysis of droop-controlled inverters for microgrid applications," *IEEE Trans.on.Smart Grid.*,vol. 5, no. 6, pp. 2980-2987, Nov. 2014.

[11] N. Pogaku, M. Prodanovic, and T. C. Green, "Modeling, analysis and testing of autonomous operation of an inverter-based microgrid," *IEEE Trans. Power Electron.,* vol. 22, no. 2, Mar.2007, pp. 613–625.

[12] Y. A. -R. I. Mohamed and E. El-Saadany, "Adaptive decentralized droop controller to preserve power sharing stability of paralleled inverters in distributed generation Microgrid," *IEEE Trans. Power Electron.,* vol. 23, no. 6, Nov. 2008, pp. 2806–2816.

[13] A. Kahrobaeian and Y. A.-R. I. Mohamed, "Analysis and Mitigation of Low-Frequency Instability in Autonomous Medium-Voltage Converter-Based Micro-Grids with Dynamic Load", *IEEE Trans. On Industrial Electronics,* vol.61, no. 4, April 2014, pp.1643-1658.

[14] R. Majumder, B. Chaudhuri, and A. Ghosh, "Improvement of stability and load sharing in an autonomous microgrid using supplementary droop control loop," *IEEE Trans. Power Syst*., vol. 25, no. 2, pp. 796–808, May 2010.

[15] E. Barklund, N. Pogaku, M. Prodanovic, C. Hernandez-Aramburo, and T. C. Green, "Energy management in autonomous microgrid using stability-constrained droop control of inverters," *IEEE Trans. Power Electron.*,vol. 23, no. 5, pp. 2346–2352, Sep. 2008.

[16] E. A. A. Coelho, P. Cabaleim, and P. F. Donoso "Small Signal Stability for Single Phase Inverter Connected to Stiff AC System," in *Proc. IEEE-IAS'99 Annu. Meeting,* 1999, pp. 2180-2187.

[17] J. M. Guerrero, L. G. de Vicuña, J. Matas, M. Castilla, and J. Miret, "A wireless controller to enhance dynamic performance of parallel inverters in distributed generation systems," *IEEE Trans. Power Electron*., vol. 9, pp. 1205–1213, Sep. 2004.

[18] J. M. Guerrero, J. Matas, L. G. de Vicu˜na, N. Berbel, and J. Sosa, "Wireless-control strategy for parallel operation of distributed generation inverters," in *Proc. IEEE ISIE Conf*., Croatia, Jun. 2005, pp. 846–850 .

[19] A. Kahrobaeian and Y. A.-R. I. Mohamed, "Analysis and Mitigation of Low-Frequency Instability in Autonomous Medium-Voltage Converter-Based Micro-Grids With Dynamic Load", *IEEE Trans. on Industrial Electronics*, vol.61, no. 4, April 2014, pp.1643-1658.

[20] N.Bottrell and T. Green, "Modelling Microgrid with active loads," in *Proc. 13th IEEE Workshop Control Model. Power Electron*, Jun. 2012, pp. 358–362.

[21] Nathaniel Bottrel, Milan Prodanovic and Timothy C. Green "Dynamic Stability of a Microgrid with an Active Load" *IEEE Transactions on Power Electronics*, Vol. 28, No. 11, November, 2013, pp. 5107–5119.

[22] F. Botteron, H. Pinheiro, H. A. Grundling, J. R. Pinheiro, and H.L. Hey, "Digital voltage and current controllers for three-phase PWM inverter for UPS applications," *IEEE IAS'01*, vol. 4, pp. 2667 – 2674, 2001.

[23] Y. Tao, Q. Liu, Y. Deng, X. Liu, and X. He, "Analysis and mitigation of inverter output impedance impacts for distributed energy resource interface," *IEEE Trans. Power Electron.*, vol. 30, no. 7, pp. 3563-3576, July. 2015.

[24] J. Kim, J. M. Guerrero, P. Rodriguez, R. Theodorescu, and K. Nam, "Mode adaptive droop control with virtual output impedances for inverter-based flexible AC microgrid," *IEEE Trans. Power Electron.*, vol. 26, no. 3, pp. 689–701, Mar. 2011.

[25] M. Belkhayat, R. Cooley, and A. Witulski, "Large signal stability criteria for distributed systems with constant power loads," in *Proc. IEEE 26th Power Electron. Spec. Conf.*, Atlanta, GA, Jun. 1995, pp. 1333–1338.

[26] G. Brandli and M. Dick, "Alternating current fed power supply," U.S. Patent 4 084 217, Nov. 4, 1978.

Wei Zhao received the B.S. degree and the M.S. degree in electrical engineering and Power Electronics and Power Drives from Yanshan University, Qinhuangdao, China, in 2006 and 2009 where he is currently working toward the Ph.D. degree in power electronics. His current research interests include the stability analysis of microgrid and power quality.

Erdong Chen received the B.S. and M.S. degree in electrical engineering from YanShan University, Qinhuangdao, China, in 2013 and 2016, respectively.

She is a R&D engineers in power electronics in Shanghai, China. Her research interests include high power converters, dc/dc converters and control in power electronics.

Xiaofeng Sun (M'11) received the B.S. degree in electrical engineering from Northeast Heavy Machinery Institute in 1993, Heilongjiang, China, and the M.S. and Ph.D. degrees in power electronics from Yanshan University, Hebei, China in 1999 and 2005, respectively.From 2003 to 2007, he was an Associate Professor with Yanshan University, where since 2008 he has been a Professor and also the Director at the Key Laboratory of Power Electronics for Energy Conservation and Motor Drive of Hebei Province. He has authored or coauthored more than 70 transactions and conference papers. His current

research interests include dc-dc converters, multiple-input converters, hybrid electric vehicles, microgrids, and power quality control.

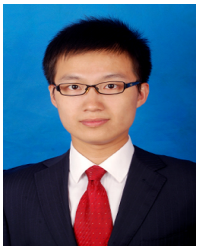

Lei Qi received the B.S. degree and the M.S. degree in electrical engineering from Yanshan University, Qinhuangdao, China, in 2014 and 2017, where he is currently working toward the Ph.D. degree in power electronics.His current research interests include the energy management, nanogrids and stability analysis.